JOURNAL OF APPLIED ELECTROCHEMISTRY 23 (1993) 19–25

Estimation of corrosion conditions of a phosphoric acid fuel cell

K. MITSUDA, T. MURAHASHI

Central Research Laboratory, Mitsubishi Electric Corporation, Tsukaguchi-honmachi 8-1-1, Amagasaki-shi, Hyogo 661, Japan

M. MATSUMOTO, K. USAMI

Kobe Works, Mitsubishi Electric Corporation, Wadasaki-cho 1-1-2, Hyogo-ku Kobe, Hyogo 652, Japan

Received 2 January 1992; revised 20 May 1992

The changes in the anode and cathode potentials in the horizontal plane of a phosphoric acid fuel cell (PAFC), under various conditions of reactant gas pressure and its utilization, were studied using a single cell with twelve reference electrodes located around the cathode. Pressure–utilization (P–U) potential maps were obtained from the data at various reactant gas partial pressures (PO_2, PH_2) and their utilization (UO_2, UH_2). These maps show the corrosion conditions clearly. A PO_2–UO_2 potential map of maximum cathode potential showed that the cathode is corroded at high oxygen partial pressures and at low oxygen utilization. Cathode corrosion can occur over the entire cell surface. A PH_2–UH_2 potential map of maximum cathode potential showed that the cathode is corroded at high hydrogen utilization and at any hydrogen partial pressure. However, in this case, cathode materials corrodes at the fuel outlet; the potential does not climb to high values at the fuel inlet area. Fuel gas flowing in series resulted in a lower possibility for corrosion than parallel gas flow.

1. Introduction

Most phosphoric acid fuel cell (PAFC) components are made of carbon. Therefore, the carbon corrosion of those components is a critical problem for the long life operation of a PAFC. Many studies have been conducted on the problem of carbon corrosion. Christner *et al.* [1] studied the corrosion of carbon plate materials. Venkatesh [2] has evaluated the corrosion resistance of substrates of electrodes. Hooie *et al.* [3] have reported the electrochemical corrosion of catalyst support. Tsutsumi *et al.* [4] reported that fuel starvation had a serious influence by causing carbon corrosion in the anode. Miki *et al.* [5] reported carbon corrosion of the anode under conditions of negative cell voltage. Recent work reported [6, 7] carbon corrosion was more often observed at the cathode side components. Platinum particles in the electrode were also dissolved by electrochemical corrosion reactions at high potential [8]. It is therefore necessary to operate so that the anode and cathode potentials are not closer than 1 V/RHE (preferably 0.8 V/RHE or less) [1–8].

Previous work reported [9, 10] the non-homogeneous distribution of polarization in the horizontal plane of a PAFC using a single cell equipped with multiple reference electrodes. Shifts in the cathode and anode potentials in the positive direction were observed in the fuel outlet area. These shifts were increased by an increase in hydrogen utilization. The RHE potential in the fuel outlet area shifted in the negative direction versus the potential of RHE in the fuel inlet area. Those results indicated that the acidity of the electrolyte of a PAFC can change locally due to increased fuel utilization. When fuel utilization increases, the cathode potential in the fuel outlet area becomes the most positive potential and cathode carbon corrosion can occur locally in the fuel outlet area. The potential shift was improved by changing the gas flow type in the horizontal plane of the cell [10].

Recent work with multiple reference electrodes reported [11] that fuel starvation occurred when fuel utilization was greater than 95%. Also, the cathode potential in the fuel outlet area shifted significantly toward the positive. Simultaneously, CO and CO_2 were detected in the air exhaust gas, pointing to carbon corrosion in the cathode components. By further increasing the fuel utilization, the cell voltage changed to negative and the anode potential in the fuel outlet area became the highest. At that time, significant amounts of CO and CO_2 were detected in the fuel exhaust gas, indicating the occurrence of carbon corrosion in the anode components.

This paper describes studies of the changes in the anode and cathode potentials in the horizontal plane under various conditions of the reactant gas pressure and its utilization using a single cell with twelve reference electrodes. Pressure–utilization (P–U) potential maps were obtained from the data at various levels of the partial pressure of reactant gas (PO_2, PH_2) and its utilization (UO_2, UH_2). These maps clearly show the corrosion conditions, and the limits of the operation conditions. As a countermeasure against corrosion,

0021-891X

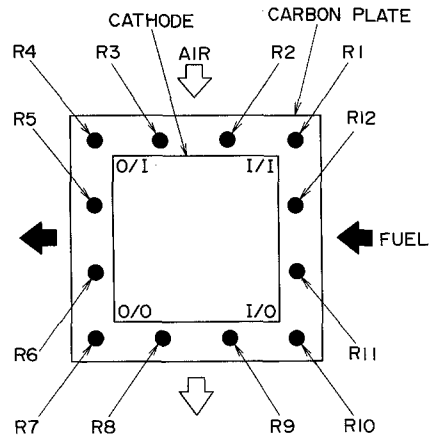

Fig. 1. The arrangement of a single cell with twelve-reference electrodes.

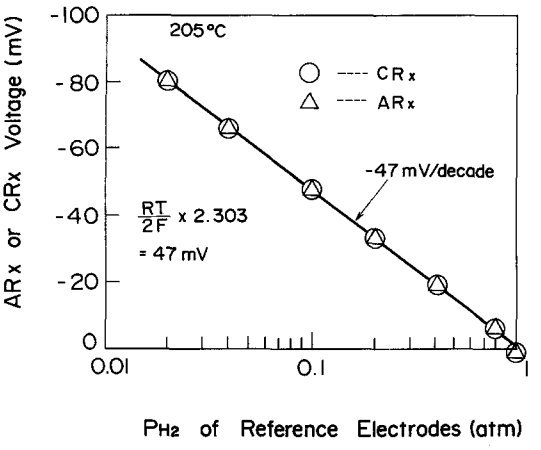

Fig. 3. Reliability test of the twelve-reference electrodes. 2.303 ($RT/2F$) = 47 mV. (○) CRx, (△) ARx.

series fuel gas flow type (serial flow type) was compared with the simplest parallel fuel gas flow type (parallel flow type) using two 18-cells large stacks. Serial flow had the effect of lowering the possibility of corrosion, which was also indicated experimentally by the P–U potential maps obtained by the single cell with twelve reference electrodes.

2. Experimental details

Figure 1 shows the location of active components and reference electrodes. The fuel and air flows are at right angles (cross-flow), and twelve reversible hydrogen electrodes (RHEs) which act as reference electrodes are disposed around the outside of the cathode. They were named R1, R2, . . . , R12 as shown in Fig. 1. In the diagram, as an example, I/O indicates the fuel inlet and air outlet corner. The effective electrode area of the cell was 100 cm^2, and the size of the reference electrodes was 0.6 cm in diameter (0.3 cm^2). Electrodes were fabricated using the reverse role coater (RRC) method [12]. The loadings of platinum supported on carbon were 0.7 mg cm^{-2} and 0.3 mg cm^{-2} for the cathode and anode, respectively.

Figure 2 shows a cross-sectional view of the cell near a reference electrode. Pure hydrogen was supplied to the reference electrodes using Teflon tubes

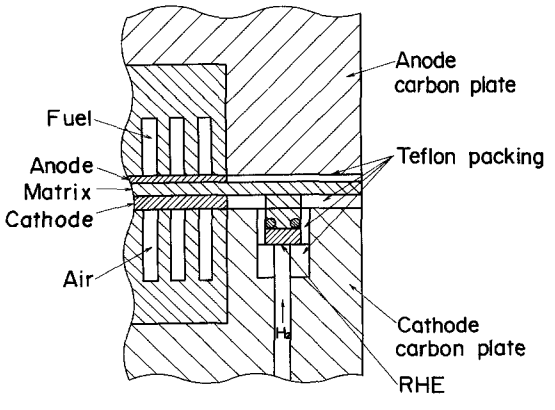

Fig. 2. Cross-sectional view showing the position of the cathode, the anode and the reference electrode.

embedded in the cathode carbon plate. Gold wire, 0.3 mm in diameter, was embedded in a Teflon tube as the lead wire from the reference electrode. The matrix sheet was made of SiC (85 wt %) and polytetrafluoroethylene (PTFE) particles (15 wt %), and was fabricated using a roller press method. The average thickness was 210 μm.

The reliability of the twelve RHEs' potential was confirmed in the following experiment. First, pure hydrogen was supplied to the cathode (referred to as C) or anode (referred to as A), and air or fuel gas (H_2 80% + CO_2 20%) was supplied to the other electrode. Then, diluted hydrogen was supplied to the twelve RHEs (referred to as Rx, x = 1 to x = 12), and the voltage between an RHE (Rx) and pure hydrogen electrode (C or A) was measured without load. In these cases, the cathode or the anode was used as a reference electrode against which to measure the twelve RHEs. The results are shown in Fig. 3, in which circles denote voltages of CRx (between C and Rx), and triangles those of ARx (between A and Rx). If there were any gas leaks or other problems with the RHEs, the overpotential would increase significantly as the hydrogen partial pressure decreased. However, the data of the twelve RHEs (ARx or CRx) under the same conditions was in an error range of 1 mV or less. Accordingly, all the data of the twelve RHEs could be included in the triangular marks or the circles in Fig. 3, even under low hydrogen pressure conditions. These results indicated that the RHEs all worked satisfactorily. The slope of the straight line in Fig. 3 was 47 mV per decade. The theoretical voltage changes due to dilution are determined by using Nernst's equation: $E_c = E_0 + (RT/nF) \ln PH_2^1/PH_2^2$. The theoretical slope, $(RT/nF) \ln PH_2^1/PH_2^2$, was calculated as 47 mV per decade ($PH_2^1/PH_2^2 = 10$) at 205° C, and this numerical value coincides with the slope of the straight line. This fact also indicated the twelve RHEs were highly reliable.

Changes in the anode and cathode potentials, under atmospheric pressure (205° C, 150 mA cm^{-2}), were investigated by varying the partial pressure of the

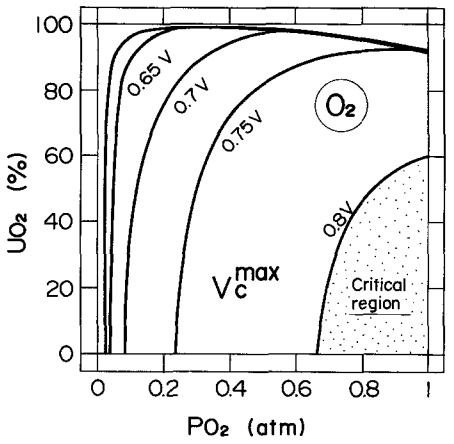

Fig. 4. PO_2–UO_2 potential map (V_c^{max}).

reaction gas (PO_2, PH_2), and the utilization of reaction gas (UO_2, UH_2). The fuel used was SRG (simulated reforming gas; H_2 80% + CO_2 20%) or a mixture gas of hydrogen and nitrogen. The oxidant used was air or a mixture of oxygen and nitrogen.

The cathode potential was corrected by adding the cell *iR* drop (ohmic loss). Ohmic loss was measured with a milliohmmeter (VP-2811A, Matsushita Communication Industry Co. Ltd).

Two short stacks of 18-cells were used in the comparison test of the serial flow type and the parallel flow type. The effective electrode area of the cells was about 3600 cm^2. The two stacks were operated under atmospheric pressure and at about 205° C. The current density was fixed at 150 mA cm^{-2}. Simulated reforming gas (SRG) or reforming gas from methane was used as the fuel, and air was used as the oxidant. The fuel utilization of the stacks was about 80%, and the air utilization was about 60% during 5000 hours of operation.

3. Results and discussion

3.1. *Influence of oxygen partial pressure (PO_2) and oxygen utilization (UO_2)*

Changes in the cathode potential and anode potential were investigated by fixing the utilization of fuel (SRG) at 75% and varying the oxygen partial pressure and oxygen utilization. As the oxygen partial pressure increased and the oxygen utilization decreased, the cathode potential increased. However, the potential distribution in the horizontal plane of the cell is less, and the difference between the maximum value (V_c^{max}) and minimum value (V_c^{min}) of the cathode potential was within 30 mV in all cases.

Figure 4 shows a potential map of PO_2–UO_2, showing the dependence of oxygen partial pressure (PO_2) on oxygen utilization (UO_2) of the cathode potential. The cathode potentials shown in Fig. 4 are the maximum cathode potentials (V_c^{max}) in the plane of the cell. In order to show corrosion conditions clearly, a 'critical region' is noted in the lower right corner of the diagram. The critical region was defined as the potential from 0.8 V to 0.9 V with respect to RHE. This critical region is estimated to extend to the middle of the diagram when the load decreases (lower current density). Furthermore, since the difference between the maximum value (V_c^{max}) and minimum value (V_c^{min}) of the cathode potential in the horizontal plane of the cell was small (within 30 mV), it is predicted that the cathode corrosion could occur over the entire cell surface. In an actual cell, air is usually used as the oxidant, the oxygen partial pressure is low, and the possibility of corrosion is low under normal operating conditions. Under low load conditions, however, when oxygen utilization is lowered, it is possible for the carrying carbon to corrode the entire cathode, and the platinum is likely to be dissolved, lowering the cell characteristics. The no load condition will increase the possibility of corrosion significantly. Since the anode potential never becomes high, there seems to be no possibility of corrosion.

To summarize the results and the discussion, three facts were ascertained from the influence of PO_2 and UO_2.

(i) The PO_2–UO_2 potential map shows that the cathode suffers corrosion at high oxygen partial pressures and at low oxygen utilization.

(ii) Because the potential distribution is small in the horizontal plane of the cell, cathode corrosion can occur over the entire cell surface.

(iii) There seems to be no possibilities of anode corrosion under any PO_2 and UO_2 conditions.

3.2. *Influence of hydrogen partial pressure (PH_2) and hydrogen utilization (UH_2)*

Changes of the cathode potential and anode potential were investigated by fixing air utilization at 50%, and varying the hydrogen partial pressure and hydrogen utilization. As hydrogen utilization increased, there was a significant shift in potential at the fuel outlet area, and a large potential distribution in the cell was observed.

Figure 5 shows the potentials of the anode and cathode at various RHE positions indicated on the *x*-axis when the hydrogen utilization was raised to 97% at PH_2 = 0.8 atm, and PH_2 = 0.043 atm. From R4 to R8, a significant potential shift occurred at the fuel outlet area, and in this region the cathode potential exceeded 0.8 V/RHE. A significant potential shift at the fuel outlet area increases the possibility of corrosion in that area. In all cases, it was observed that the potentials of the RHE in the fuel outlet area shifted negatively compared with RHE in the fuel inlet area when the potential of the anode and cathode shifted. The potential shift of RHE always shifted to the same degree as the potential shift of the anode and cathode.

Figure 6 is a potential diagram which explains the mechanism of the potential shift. Figure 6(a) and (b) show the potentials of the cathode, the anode, and RHE potentials (which are equal to the oxidation potential of hydrogen (H^+, H_2) at each position) using the results in Fig. 5. The calculated oxygen reduction potential (O_2, H^+/H_2O) is also given. Figure 6(a) is

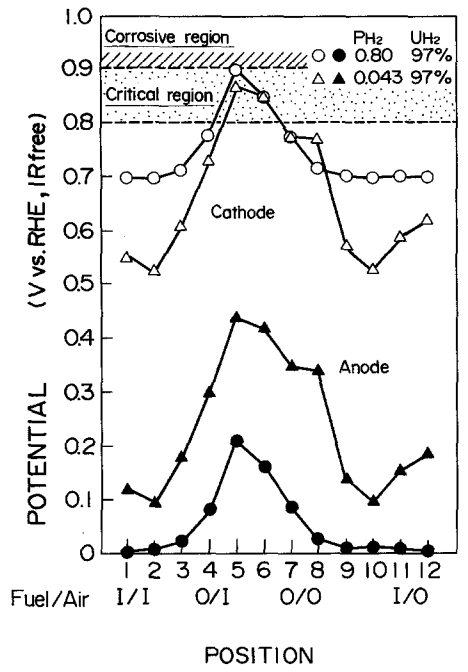

Fig. 5. Influence of hydrogen partial pressure on the cathode and anode potentials in the horizontal plane of the cell.

based on the 'electrolyte potential' or 'electrochemical potential' because the RHE potentials in the horizontal plane are constant. On the other hand, Fig. 6(b) is based on the 'electrode potential' or 'electric potential' because the anode and cathode potentials in the horizontal plane are constant. In Fig. 6(a), the RHE potentials are constant, and the cathode and the anode potentials in the fuel outlet area shifted significantly in the positive direction. On the other hand, in Fig. 6(b), the anode and cathode potentials are constant, and the potentials of hydrogen oxidation (H^+/H_2) and oxygen reduction (H^+, O_2/H_2O) drop from the inlet to the outlet area. Since the redox potential of

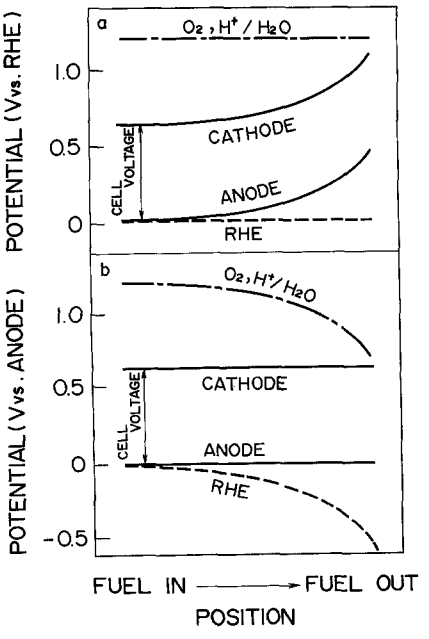

Fig. 6. Potential changes from fuel inlet to fuel outlet during violent potential shift (a: based on the 'electrolyte potential', b: based on the 'electrode potential').

H^+/H_2 or H^+, O_2/H_2O changes with the pH of the electrolyte (the change is 59 mV/pH at 25° C and 95 mV/pH at 190° C [13]), the electrolyte is less acidic in the fuel outlet area than in the inlet area. At equibrium, the electrochemical and electric schemes must coincide in the horizontal plane of a cell due to migration of electrons and protons. However, the two schemes in Fig. 6 disagree. If the volume of the solution is large enough, protons will soon be supplied from the surroundings and the potential shift will be cancelled. However, a fuel cell is very thin for its wide area, and protons do not move easily in the horizontal direction. Therefore, due to the fuel cell composition, proton movement is restricted, and the potential shift is maintained. The use of a single cell with multi-reference electrode unveils the mechanism of potential shift. The influence of the potential shift (E_{sh}) on both the cathode and anode potentials (E_c, E_a) can be defined quantitatively by the following equations [10].

$$E_c(\text{V/RHE}) = E[H^+, O_2/H_2O] + (RT/2F) \times (\ln(PO_2^{1/2}/PH_2O)) - \eta_c + E_{sh} \quad (1)$$

$$E_a(\text{V/RHE}) = E[H^+/H_2] - (RT/2F) \times (\ln(PH_2)) + \eta_a + E_{sh} \quad (2)$$

$$E_{sh}(\text{V}) = (RT/F)\Delta \ln(H^+) = 2.303(RT/F)\Delta\text{pH} \quad (3)$$

where η_c and η_a are the overpotentials of the cathode and the anode, respectively. It should be noted that, when the pH (Ho) changes by 1, the RHE potential changes by 95 mV at 205° C. If the pH of the electrolyte is constant in the horizontal plane of a cell, E_{sh} is zero. If the pH of the electrolyte changes locally in the fuel outlet area, E_{sh} becomes positive, and the cathode potential increases in that area. Therefore, η_c in the fuel outlet area should decrease compared with that in the fuel inlet area. This indicates a change in the current distribution, that is, current convergence in the fuel inlet area. Though data on the acidity of concentrated phosphoric acid at high temperatures is limited, Dowing *et al.* [14] reported the acidity at 25° C to 27° C as $Ho = -4.8$; at 100% H_3PO_4, where Ho is the Hammet acidity function. Hence, concentrated phosphoric acid is a 'super acid', and at high temperatures, phosphoric acid must be a stronger 'super acid' the same as the case of concentrated sulphuric acid. If the acidity of the electrolyte in the fuel outlet area changes locally from $Ho = -5$ to $Ho = 0$, E_{sh} becomes 0.48 V. This value is large enough to explain the significant potential shift in Fig. 5.

Figure 7 shows the hydrogen utilization dependence of the maximum cathode potential (V_c^{max}), and Fig. 8 is a PH_2–UH_2 potential map of these results. At any hydrogen partial pressure, when the hydrogen utilization increases, the maximum cathode potential exceeds 0.9 V RHE, and a high possibility of corrosion is suggested. The 'corrosive region' in Fig. 7 was defined as the region exceeding 0.9 V/RHE. However, the cathode potential at the fuel inlet area remained at a low level. Therefore, the cathode near the fuel outlet

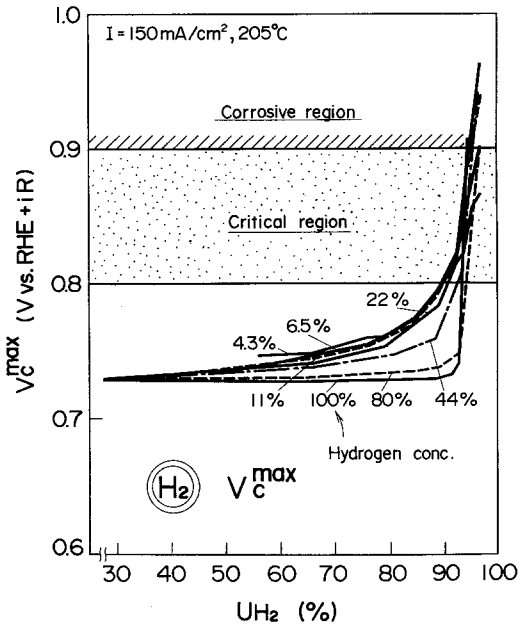

Fig. 7. Hydrogen utilization dependence of maximum cathode potential (V_c^{max}).

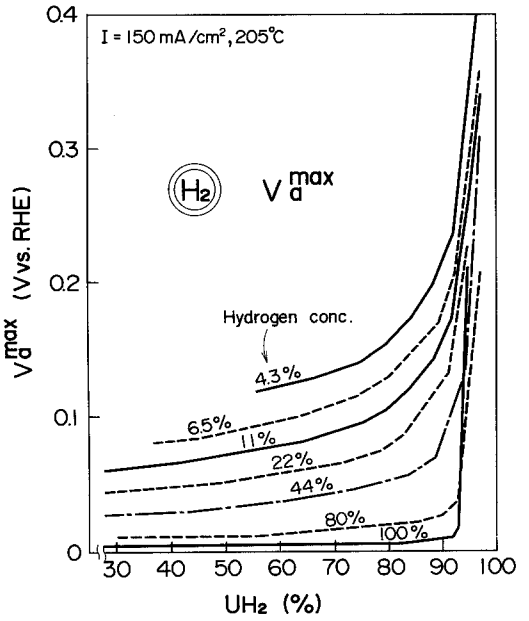

Fig. 9. Hydrogen utilization dependence of maximum anode potential (V_a^{max}).

corrodes, and the potential near the fuel inlet does not increase much.

The hydrogen utilization dependence of the maximum potential (V_a^{max}) and the PH_2–UH_2 potential maps are shown in Figs 9 and 10, respectively. Similarly, these results suggest that the possibility of corrosion is very high when hydrogen utilization is at a high level. At very high hydrogen utilization levels, the cell voltage was negative. In an actual stack a negative stack voltage is not possible. However, it is possible that one or two cells in a stack change to a negative voltage under undesirable operating conditions. Under normal operating conditions, the hydrogen utilization of fuel is about 80%, but it is very possible that substantial hydrogen utilization may temporarily exceed 90% due to load fluctuations, variations in the composition of reforming gas, and changes in fuel flow rate. This would cause the cathode near the fuel outlet area to corrode.

The influence of PH_2 and UH_2 can be summarized as follows.

(i) The PH_2–UH_2 potential map of maximum cathode potential shows that the cathode is corroded when hydrogen utilization is high and at any hydrogen partial pressure.

(ii) Because the potential shift is located in the fuel outlet area, cathode corrosion can occur near the fuel outlet area.

(iii) the PH_2–UH_2 potential map of maximum anode potential shows that the anode is also corroded when hydrogen utilization is high and at any hydrogen partial pressure; however, at a negative cell voltage.

3.3 *Countermeasures against corrosion*

Low load or no-load (open circuit) PO_2 and UO_2 operation conditions will significantly increase the possibility of corrosion of the cathode. Thus, cathode corrosion can be prevented by increasing oxygen utilization or reducing oxygen partial pressure.

In order to raise the efficiency of the fuel cell, the operating conditions of PH_2 and UH_2 must not be made so that hydrogen utilization is elevated. It is, of

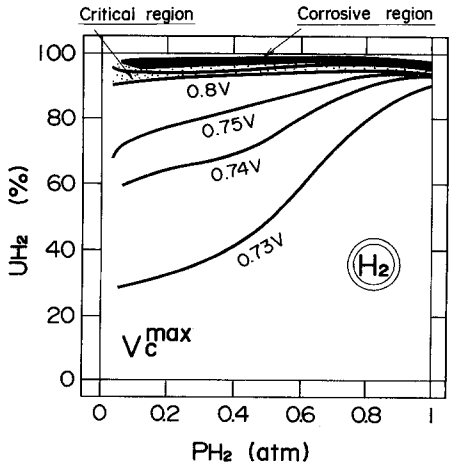

Fig. 8. PH_2–UH_2 potential map (V_c^{max}).

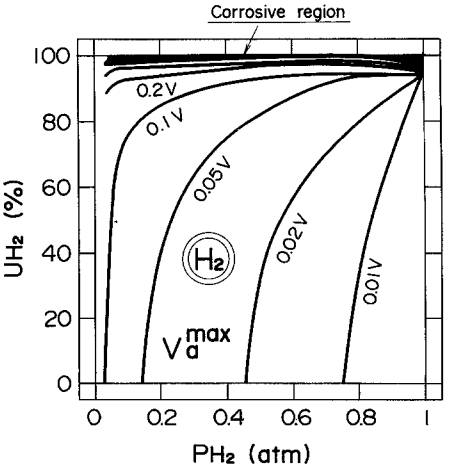

Fig. 10. PH_2–UH_2 potential map (V_a^{max}).

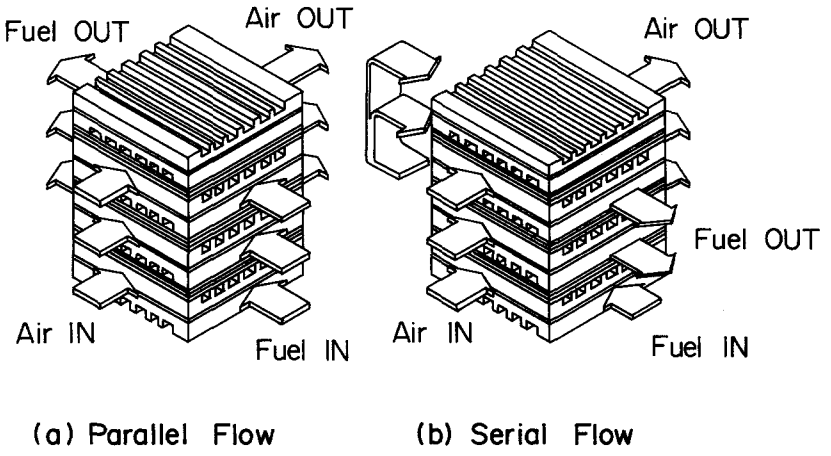

Fig. 11. Comparison of fuel gas flow types; (a) parallel flow type, (b) serial flow type.

course, impossible to utilize hydrogen near 100%, but from Fig. 8, it is apparent that enough countermeasures must be taken so that the critical region or corrosive region near 100% is not reached. We investigated the differences in potential behaviour using a reactant gas flow system in a single cell with multiple reference electrodes, and found that, compared with the simplest cross flow, a fuel return flow, co-flow and counter flow were effective in narrowing the critical region and corrosive region [10]. These cell compositions are, however, too complicated to be used in practice. As a result of further studies, it has been found that the serial flow system, which returns fuel gas in the direction of laminations within the stack, is a simple and effective method of preventing corrosion.

Figure 11 compares the gas flow in a stack between the parallel flow type and the serial flow type. In the serial flow type, fuel is first fed in to the upstream cell, then, the residual fuel not consumed by the upstream cell is supplied to the downstream cell. The upstream cell, also carries the fuel to be supplied to the downstream cell, therefore, the ratio of fuel used to fuel supplies to the upstream cell is substantially lower than the parallel system. In addition to the fuel supplied to the downstream cell, it receives fuel not consumed in the upstream cell, therefore, the ratio of fuel used to fuel supplied to the downstream cell is also substantially lower than the parallel system. Hence, in the serial flow type, hydrogen utilization may be substantially lowered both in the upstream and in the downstream cells. Of course, the hydrogen partial pressure of the fuel supplied to the downstream cell is lower than that in the upstream cell, however, as is revealed in Fig. 8, the possibility of corrosion is not increased substantially if the hydrogen partial pressure drops. In addition, the hydrogen partial pressure of the fuel is much higher than the oxygen partial pressure in the air, therefore, the cell voltage is not lowered as much if the hydrogen partial pressure drops a little.

Figure 12 shows the deterioration over time of the parallel flow type and serial flow type when two large, 10 kW class, 18-cells stacks were employed. The results prove that the serial flow type does not deteriorate as rapidly as the parallel flow type.

More specifically, in the parallel flow type, every time the ratio of fuel used to fuel supplied increases, as experienced during normal operating conditions, the performance of the cathode may be lowered due to corrosion of the cathode carbon or the dissolution of the platinum catalyst in the cathode. These conditions are avoided in the serial flow type.

To summarize, it was found, both from a comparison test of two stacks and from a theoretical consideration, that there is a lower possibility of corrosion in the serial flow type than the parallel gas flow type.

4. Conclusions

The PO_2–UO_2 potential map of maximum cathode potentials shows that high oxygen partial pressures and low oxygen utilization are conditions leading to corrosion of the cathode. Since the difference between the maximum value (V_c^{max}) and the minimum value (V_a^{min}) of cathode potentials in the horizontal plane of the cell was small (within 30 mV), it is predicted that cathode corrosion could occur over the entire cell surface.

Increasing UO_2 or reducing PO_2 is a countermeasure for cathode corrosion. On the other hand, there seems to be no possibility of anode corrosion at any PO_2 or UO_2.

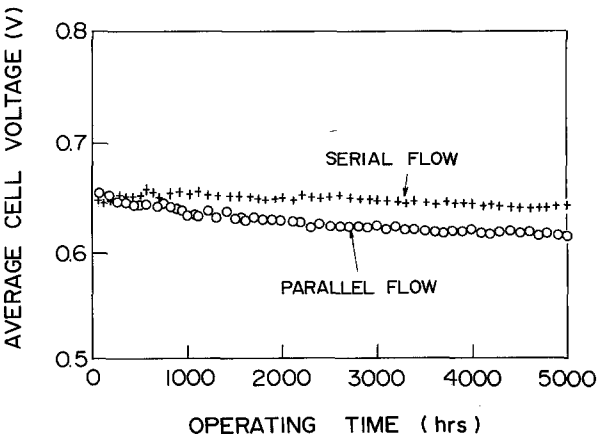

Fig. 12. Ageing characteristics of 18-cells large size stacks.

The PH_2–UH_2 potential map of maximum cathode potentials shows that operation at high hydrogen utilization and at any hydrogen partial pressure places severe corrosion conditions on the cathode. The PH_2–UH_2 potential map of maximum anode potentials shows that the anode is also subject to corrosion at high hydrogen utilization and at any hydrogen pressure; however, at a negative cell voltage. Thus, the anode corrodes only at negative cell voltages. Since the potential shift was localized in the fuel outlet area, the corrosion of the cathode will also occur near that area.

Decreasing UH_2 is a countermeasure for cathode or anode corrosion. Serial fuel gas flow results in a lower possibility of corrosion than parallel gas flow.

References

[1] L. G. Christner, H. P. Dhar, M. Farooque and A. K. Kush, *Corrosion* **43** (1987) 571.

[2] S. Venkatesh, CORROSION/86, paper no. 82, National Association of Corrosion Engineers (NACE), Houston, TX (1986).

[3] D. T. Hooie and E. H. Camara, CORROSION/86, paper no. 83, NACE, Houston, TX (1986).

[4] Y. Tsutsumi, I. Sone and Y. Nanba, '86 Fuel Cell Seminar, Abstracts (1986) p. 110.

[5] A. Miki, S. Uozumi, Y. Tsutsumi and K. Nanba, Spring Meeting of Electric Engineers of Japan, Abstracts no. 1226 (1987).

[6] K. Mitsuda, H. Shiota and T. Murahashi, *Corrosion* **46** (1990) 628.

[7] M. Farooque, A. Kush and L. Christner, *J. Electrochem. Soc.* **137** (1990) 2025.

[8] P. Bandra, S. J. Clouser and E. Yeager, *ibid.* **126** (1979) 1631.

[9] K. Mitsuda and T. Murahashi, *ibid.* **137** (1990) 3079.

[10] K. Mitsuda and T. Murahashi, *J. Appl. Electrochem.* **21** (1991) 395.

[11] K. Mitsuda and T. Murahashi, *ibid.* **21** (1991) 524.

[12] K. Mitsuda, I. Hirata, H. Miyoshi and K. Kitazaki, *U.S. Patent 4 603 060* (1986).

[13] M. Pourbaix, 'Atlas D'Equibres Electrochimiques', Cauthier–Villars, (1963) p. 102.

[14] R. G. Dowing and D. E. Peason, *J. Am. Chem. Soc.* **83** (1961) 1718.